Applied Thermal Engineering 31 (2011) 3761–3767

Contents lists available at ScienceDirect

Applied Thermal Engineering

journal homepage: www.elsevier.com/locate/apthermeng

Experimental evaluation of cell temperature effects on miniature, air-breathing PEM fuel cells

Z. Williamson [a], Daejoong Kim [b,*], Dae-Keun Chun [a], Tonghun Lee [a], Cody Squibb [a]

[a] Michigan State University, Engineering Research Complex, East Lansing, MI 48823, USA
[b] Sogang University, 1 Shinsu-dong, Mapo-gu, Seoul 121 742, Republic of Korea

ARTICLE INFO

Article history:
Received 15 March 2011
Accepted 7 June 2011
Available online 14 June 2011

Keywords:
Air-breathing
PEM fuel cell
Temperature effects
Air buoyancy

ABSTRACT

The impact of temperature on air-breathing, polymer electrolyte membrane (PEM) fuel cells is investigated using polarization and impedance spectroscopy. Three active area sizes of 5 cm^2, 10 cm^2, and 25 cm^2 in both forced convection and air-breathing cathode configurations are presented. The cell design incorporates a large thermal body which can conduct heat away from the active membrane area and minimize the influence of self-heating; allowing for active and precise control of temperature regardless of the current density. Polarization and electrochemical impedance spectroscopy (EIS) results show that at higher current densities, elevated temperature increases the buoyancy of the air around the cell, which improves the air-breathing fuel cell performance. However, the opposite is true for lower current densities as membrane dehydration becomes more prevalent at higher temperatures. Temperature plays a larger role in air-breathing fuel cell performance than the actual size of the cell, whereas both cell temperature and size influence the cell performance for forced convection fuel cells. The discussions presented here provide guidelines for thermal engineering of practical air-breathing fuel cells as a promising portable energy source for the future.

1. Introduction

While the concept of using fuel cells for power generation has been proposed for decades, the interest in their development as a widely adopted alternative energy source has been receiving significantly increased attention in recent years as the search for greener and more efficient energy technologies becomes ever more important. Among the many fuel cell types, the polymer electrolyte membrane (PEM) fuel cells are thought to be one of the more effective power options for future use in cars and small scale applications because of their relatively low operating temperature, high energy density, and high efficiency [1–3].

In the lower power, portable electronics domain, batteries have and continue to dominate as the practical power supply of choice. Fuel cells however, may one day replace batteries in this category and are actively being researched for this purpose. Fuel cells have higher efficiencies and while batteries “die” after a relatively short amount of time, fuel cells can continue generating power indefinitely as long as the necessary reactants are supplied. Additionally, the energy density for a hydrogen fuel cell can greatly exceed that of even a high-end Li-ion battery [2].

The PEM fuel can be configured with a forced convection cathode side for active supply of oxygen or scavenge oxygen from the atmosphere in an air-breathing design. An air-breathing fuel cell is one in which the membrane is exposed at the cathode side and oxygen is absorbed passively through free convection from the surroundings [4]. Variations of air-breathing PEM (ABPEM) fuel cells include planar and ducted cathode designs. Planar cells have cathode designs that are flat and without protrusions and the gas diffusion layer (GDL) is exposed directly to the ambient air. Ducted fuel cells have a chamber(s) through which air flows naturally over the GDL [5]. Generally, the air-breathing cathode fuel cells are less efficient than the forced convection counterpart but offer some distinct advantages for small scale portable applications (*i.e.*, cell phones or laptops). Namely, air-breathing PEM fuel cell designs are smaller, simpler in design, and only require the supply of hydrogen, as the oxygen is scavenged from the air.

In order for fuel cells to gain ground as practical power sources that are able to replace batteries, extra equipment will have to be removed from the fuel cell system including heaters, fans, humidifiers, and complicated oxidizer supply and storage units. While these are generally used to enhance the performance of a fuel cell, they add to the size of the cell and use valuable electricity produced

* Corresponding author. Tel.: +82 2705 8644; fax: +82 2712 0799.
E-mail address: daejoong@sogang.ac.kr (D. Kim).

1359-4311/$ – see front matter © 2011 Elsevier Ltd. All rights reserved.
doi:10.1016/j.applthermaleng.2011.06.010

by the cell [4,6]. It is important that they be discarded without sacrificing significant amounts of power output. This study strives to compare the performance of various forced convection PEM fuel cells and ABPEM fuel cells under practical conditions.

Performance of an ABPEM fuel cell is greatly limited by oxygen mass transport at higher current densities [7,8]. Because of this and the high activation energy needed for the oxygen reduction reaction, it is important to understand the effects that cathode design and configuration have on the fuel cell performance [5]. In addition to geometry, ABPEM fuel cells are extremely sensitive to temperature over their entire operation range. Higher temperatures can increase chemical reaction and transport rates, resulting in enhancement of the overall performance. However, higher temperatures can also lead to increased thermodynamic losses and membrane dehydration [6,9,10]. The surrounding air temperature adjacent to the GDL is also critical as it influences air buoyancy which often has a direct impact on cell performance [7,11]. The heat is mainly generated in the PEM fuel cell from the chemical reactions in a process referred to as 'self-heating,' and the impact of temperature rise from this effect is particularly important for ABPEM cells where thermal diffusion to the atmosphere is more pronounced. A number of studies have explored the impact of atmospheric conditions on fuel cell performance [8,11,12], but a systematic study of the thermal impact on an air-breathing fuel cell with controlled thermal loading has yet to be completed. Understanding the complex interaction between temperature and ABPEM fuel cell performance will be the main objective of this study.

In so doing, the performance of fuel cells in both forced convection and air-breathing configurations are compared. The three active area sizes for evaluation are: 5 cm^2, 10 cm^2, and 25 cm^2. The performances for the two operating configurations will be evaluated at various temperatures for each size, using controlled heating of the cell blocks. Self-heating is a difficult aspect of fuel cell operation to control because the heat produced by the reaction is proportional to the cell's operating current [10,11]. Previous studies have used 'self-heating' as part of the method to maintain constant cell temperature [6]. Our study is unique in that we are able to test specific cell temperatures for an air-breathing fuel cell by using both a large thermal mass which allows for very high rates of heat removal from the active area and an external heating system that was incorporated into the fuel cell to maintain both the required and elevated temperature conditions.

2. Experimental setup

Typically, the term "PEM fuel cell with air-breathing" refers to a fuel cell which uses free convection to obtain its oxygen through a cathode that is exposed directly to ambient air. In this study the free convection cells and the cells that are fed with stored oxidant both operate on air. To eliminate confusion and ambiguity, free convection cells and their performance will be referred to as "open-cathode cells" or "open cells." Similarly, the term "PEM fuel cell with forced convection" refers to the fuel cells fed air with forced convection and their performance will be termed "closed cathode cells" or "closed cells" throughout this manuscript.

2.1. Closed fuel cell

Each test cell, with the exception of the area and configuration of the serpentine flow channels, was constructed in the same way, as shown in the diagram of Fig. 1 (right) and the photo of Fig. 2 (right). Starting from the outside, the anode side of the closed fuel cell consists of an aluminum base plate (a), a gold-plated electrode (b), and a graphite Poco block with machined serpentine flow channels (c). The cathode half of the cell contains the same components. Inserted between the two halves are the gaskets (d) and membrane electrode assembly (MEA) (e in Fig. 1). Each base plate is fitted with Swagelok gas supply and vent fittings, a cartridge heater cavity, and a thermocouple port for active control of temperature. A short 3/16 inch diameter section of Nafion tubing with a rubber gasket connects the gas supply ports between the base plate and graphite blocks through a hole in the electrode. Connected to each electrode are a load lead and a sense lead. The closed fuel cell uses a 0.010 inch Teflon gasket on either side of the MEA. The cell is held together by eight ¼-28 bolts each with a torque of 50 in-lbs.

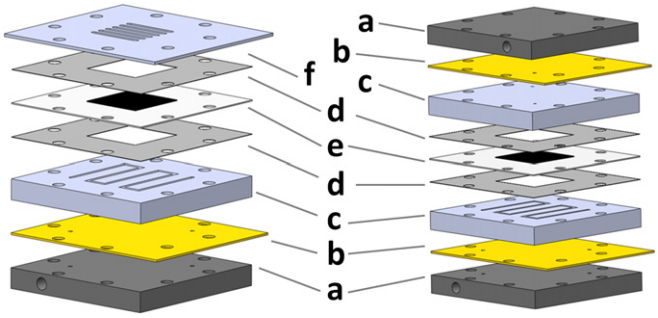

Fig. 1. Exploded view of the open-cathode, air-breathing fuel cell (left) and closed fuel cell (right).

2.2. Open-cathode fuel cell

A diagram and a photograph of the open-cathode fuel cell are shown in Fig. 1 (left) and Fig. 2 (left) respectively. The open-cathode fuel cell uses the same three anode components as the closed cell (a, b, c in Fig. 1). The cathode half of the closed fuel cell is replaced by a slotted cathode plate (f) which exposes approximately 50% of the MEA to the atmosphere. The electrode portion of the cathode top plate is gold-plated where it is in contact with the MEA and the leads.

The open-cathode plate is 1/16 of an inch thick and subsequently is not as stiff as the cathode half of the closed cell. Because of this, the same contact pressure on the MEA cannot be achieved with the open cell as with the closed cell. During initial tests, it was found that the performance of the open cell was not significantly improved when the bolt torque exceeded 10 in-lbs. Thus, in all open cell testing, the bolt torque is set to 10 in-lbs whereas the closed cell

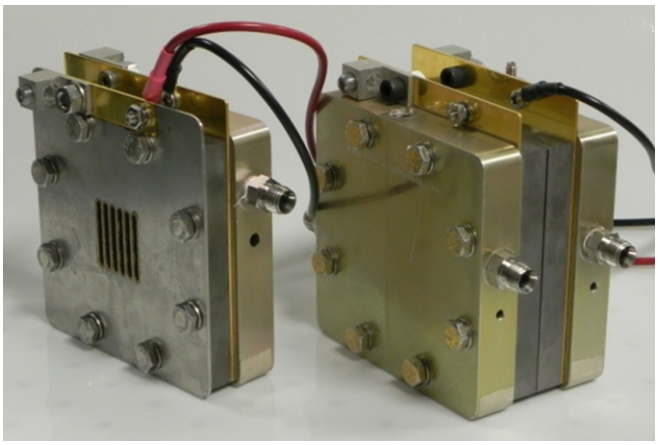

Fig. 2. Photos of open cell (right) and closed cell (left).

bolt torque is set to 50 in-lbs. In an effort to salvage some of the contact pressure lost with the open cell, the total gasket thickness was reduced. The gaskets used are 0.010 inch silicon rubber on the anode side and 0.006 inch Teflon. The silicon gasket is used to create a better hydrogen seal with lower bolt torque.

Between the aluminum base plate and graphite block, there is a Teflon gasket to electrically separate the two components. The base plates are 6061-T6 aluminum alloy with an alodine 1200 chromic coating. The graphite block is AFX-5Q pyrosealed Poco graphite. The current collectors are printer's copper with a nickel base plating and a 0.0003–0.0005 inch gold electroplating. The air-breathing cathode plates are 316 stainless steel with the same gold plating as above for electrical and electrode contact points.

The MEA's for each cell size are identical except for the active area. They were manufactured by BCS Fuel Cells. They are 5-layer, HP-A Nafion 212 self-humidifying MEA's with 0.5 mg/cm platinum loading for both the anode and cathode. The MEA's were conditioned for 10 h each in a closed cell configuration prior to testing. The cell temperature was held at 60 °C and the hydrogen and oxygen flow rates were held at 2× and 3× stoichiometry respectively and both at a gas humidifying temperature of 60 °C.

2.3. Test setup and equipment

The overall test cell setup is shown in Fig. 3. All test equipment and fuel cell operations were integrated through a LabView interface and automated. Gas flows were regulated using MKS RS485 Type 1179A mass-flow controllers. Depending on the desired test conditions, the gases can be bypassed or fed through heated humidity bottles (Fuel Cell Technologies, Inc., Albuquerque, NM). Temperature controllers monitored the cell temperatures and humidity temperatures using Ω T-type thermocouples. The fuel cell operating point was regulated with an Agilent N3304A 60A DC electronic load. It was attached to the fuel cell in a four-wire set up and used a TDK Lambda HWS300-5 power supply. The data was collected using a NI 488.2 PCI-GPID Card and a NI SCB-68 Junction box.

3. Experimental procedures

3.1. Polarization testing

For each cell size, the polarization curves were sequentially generated in potentiostatic mode to compare the overall performance. The cell was first operated at room temperature – held at open cell voltage (OCV) for 10 min and then at 0.7 V for an additional 10 min. After this, the cell temperature was raised to 30 °C and the voltage was controlled to remain steady for 10 min at a constant voltage at 0.7 V. After this sequence in the initial 30 min, the polarization test for 30 °C was started. The polarization test was completed in a constant voltage mode, starting at 0.95 V and decreasing 0.025 V every 5 min down to 0.15 V. Then the cell was held at 0.6 V for 5 min after which this cycle was restarted for the next temperature in the scan. During initial polarization testing, it was found that tests completed in potentiostatic mode were more reliable than those in galvanostatic mode for the open cells. The polarization curves generated from the potentiostatic data help to illustrate the importance of adequate membrane hydration which will be discussed in Section 4.

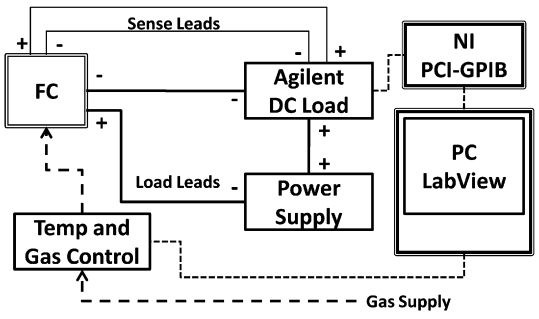

Fig. 3. Test setup for fuel cell operation.

When polarization plots were generated for closed H_2/Air operation in the constant voltage mode, the performance was very unstable. This was due to fact that the air flow controller program is based on current and in the constant voltage mode the flow control must continually iterate to give an airflow output. In the closed cell mode, this process proved to be very unstable and resulted in fluctuations in the current and instability in the air flow. To avoid this issue, polarization curves were completed in the constant current mode for the closed test cells. The data collection started at zero current density and increased at intervals of 125 mA until the voltage reached 0.2 V.

During polarization data collection, anode hydrogen flow was set to 1.5× stoichiometry for both open and closed cells with minimum flows set to 15, 30, and 75 sccm. In the closed cell mode, the cathode air flow was set to 2× stoichiometry with minimum flows of 30, 60, and 125 sccm.

3.2. Electrochemical impedance spectroscopy

A current density of 0.4 A/cm^2 was chosen for the electrochemical impedance testing because each cell was able to achieve this set point. Additionally, this current density was relatively close to where each cell configuration reached its maximum power density. The cell temperature was set and allowed to reach steady state at OCV. Then the current was allowed to reach steady state at which point the impedance data was recorded in constant current mode. The frequency scan ranged from 10 kHz to 0.1 Hz at 10 points/decade. The amplitude of the current modulation used was 10% of the DC current.

4. Results and discussion

4.1. Polarization curves

Polarization curves allow for the comparison of temperature on the overall performance of each test cell configuration. It is important to understand the behavior of the fuel cell in each of the three regions of a fuel cell polarization curve – activation, Ohmic, and mass transport [13]. This information helps to characterize the influence of temperature on cell size and configuration throughout the operational spectrum of the fuel cell. With the polarization curves, in conjunction with power density data, it becomes easier to identify where along the curve temperature either enhances or hinders performance. Note that open cell curves were generated in potentiostatic mode while closed cell data was taken in galvanostatic mode. Refer to the discussion in Section 3 for further clarification on these procedures.

4.1.1. Self-heating effects

This study focuses on cell performance at specific cell temperatures which requires that the cell temperature remain constant during testing. For our purposes, self-heating was neglected when there was not a significant (less than 1 °C) rise in cell temperature above the set point. Due to self-heating beyond the cell temperature set point, the 25 cm^2 cell could not be used in the cell size comparison along with the smaller cells. Despite the use of a high

thermal capacity cell structure, it could not shed the heat generated from the MEA fast enough to maintain constant temperature at higher current densities. Fuel cell temperature and polarization data for the 25 and 10 cm^2 open cells can be seen in relation to current density in Fig. 4a and b respectively. Fig. 4a shows the self-heating of the 25 cm^2 cell whereas self-heating does not occur for the 10 cm^2 cell in Fig. 4b.

During polarization testing of the 5 cm^2 and 10 cm^2 cells, there was no evidence of self-heating and cell temperature was maintained by the temperature controller and heater embedded in the base plate. The absence of self-heating effects for these two cells is largely due to two related factors 1) the highest current produced is relatively low and 2) the ratio of the active area to the total mass of the largely aluminum cell is small [14]. With this, any heat produced by the chemical reaction is easily conducted away from the active area, dissipated throughout the solid mass of the cell, and then leaves the cell via convection. This is discussed by Zhang and Pitchumani [15].

For the 25 cm^2 open cell, this is not the case. Here, the highest current produced is significantly larger than that of the two smaller cells and the ratio as described above is much smaller. The 25 cm^2 open cell experiences self-heating because there is more heat produced due to the higher current which cannot be shed as quickly from the cell. During the 30 °C and 40 °C polarization tests for this cell, the cell temperature began exceeding the set point temperature as current density increased. This occurred around 0.4 and 0.6 A/cm^2 for 30 °C and 40 °C, respectively, with a maximum self-heating temperature of 37 °C and 45 °C for each test. Therefore, data for the 25 cm^2 cell was not comparable with the results for the other cell sizes because the performance of the cell increased at higher current densities as the self-heating temperature increased. Normally, as will be discussed below, cell voltage drops off rather quickly with increased current density once the cell is operating in the mass transport region and the cell is increasingly starved of oxygen. In the case of the 25 cm^2 cell, the mass transport region begins at around 0.3 A/cm^2. It can be seen in Fig. 4a, that in this region for each temperature, voltage decreases more linearly with increased current density. This is assumed to be because an increase in buoyancy of the air around the cell due to self-heating increases the airflow over the cathode surface. Although exploring the effects of self-heating was not the purpose of this study, the data from the 25 cm^2 polarization testing illustrates the potential benefit of harnessing the self-heating phenomenon.

4.1.2. Temperature scan

Although an increase in temperature generally decreases kinetic losses, it is seen that at higher temperatures and lower current densities, membrane dehydration significantly outweighs the positive effects of the added heat [13]. This is most easily observed in the polarization temperature scans in Fig. 5. For dry gas, at higher

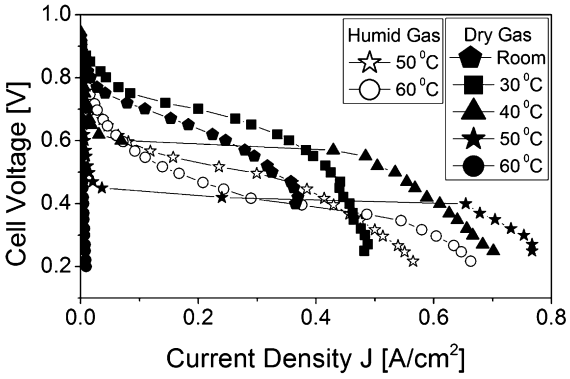

Fig. 5. Polarization curves for a temperature scan of the 5 cm^2 open cell.

cell temperatures, a significant drop in the curve is observed in the lower current density region. The performance at low current densities is very poor and the current density increases very little with each step in voltage. In this kinetic region there is little product water and the membrane is very dry [16], resulting in problems with the activation of the MEA. However, there is a critical current density between 0.03 and 0.05 A/cm^2 at which the cell begins producing enough water and the membrane very quickly becomes hydrated resulting in a dramatic jump in cell performance [10]. From observing Fig. 5, this critical current density range seems to be independent of cell temperature. At 60 °C, the membrane is too dry to reach the critical current density and the cell is not able to produce a significant amount of current. For comparison, 50 and 60 °C the polarization testing using humidified hydrogen gas is also plotted to show that poor performance in the Ohmic region is not observed where there is no drying issue in the membrane. It should be noted that when compared to the dry gas data, the humidified data show better performance at low current densities but worse performance at high current densities, as described by Jeong et al. [8].

For dry gas, at higher temperatures and low current densities, performance is poor because limited water production cannot effectively hydrate the membrane. The upper limit of the current density is extended, however, as water production increases [17]. For open cells operating in the mass transport region (higher current density), the supply of oxygen to the MEA becomes the major limiting factor on performance. However, as cell temperature increases, the air around the cell becomes more buoyant due to the increase in temperature gradient between the air near the GDL and the ambient air. This creates an updraft of air and its velocity increases with temperature, allowing for influx of more oxygen to the MEA, resulting in higher sustainable current densities [11,12,15].

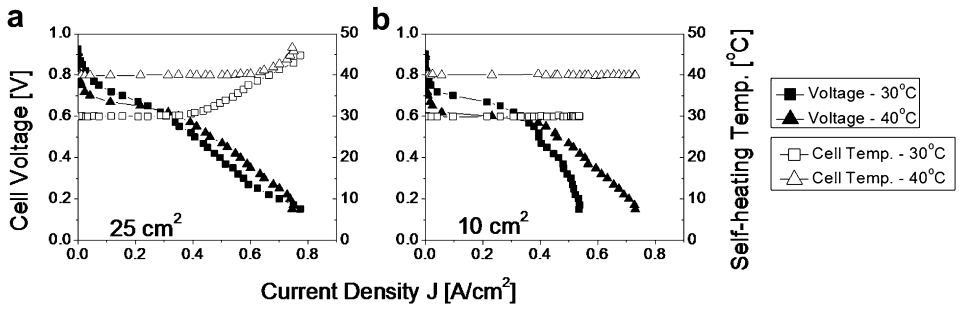

Fig. 4. Polarization curves for the a) 25 cm^2 and b) 10 cm^2 open cells. Right axis shows cell temperature. Self-heating is evident for the 25 cm^2 open cell in a).

Fig. 6 shows potential curves for open and closed cell configurations each at 30 °C and 40 °C. As previously mentioned, open cell potential curves were generated in a galvanostatic mode and closed cell curves were generated in a potentiostatic mode. Although these are not entirely comparable at individual points on the curve, they are sufficient for a comparison of the overall cell performance. In Fig. 6a, the curves show data for the open 5 cm^2 and 10 cm^2 cells at 30 and 40 °C. It was observed that in an open cell configuration, performance is more dependent on cell temperature than cell size as the curves for each temperature are essentially the same. Fig. 6b shows that in the closed cell configuration, the trend is the opposite. The curves show that at 40 °C, each cell size can produce higher current density than at 30 °C. However, the data shows that closed cell performance is more dependent on cell size than on cell temperature. This is likely due to the fact there are some cell operational characteristics that do not scale exactly with cell size such as flow losses in the gas feed channels or membrane contact pressure. Both the 5 cm^2 and 10 cm^2 fuel cells have a single serpentine flow channel in the graphite block for the delivery of gases. Because it must cover twice the area than the 5 cm^2 cell, the channel is much longer for the 10 cm^2 cell. However, the channel width and channel depth are identical for both cells suggesting that the losses in the flow channels are perhaps greater in the 10 cm^2 cell.

From the temperature scan polarization tests, we are able to realize that increased temperature decreases performance at low current densities but increases performance at higher current densities. This enhanced performance is attributed to better membrane hydration at higher current densities and more air flow across the cathode with elevated temperature. In an open-cathode configuration, performance is more heavily influenced by cell temperature than by cell size. Although performance differences for all four curves are not overly significant for the closed cell, the data suggests that size and temperature have more of an equal influence on cell performance.

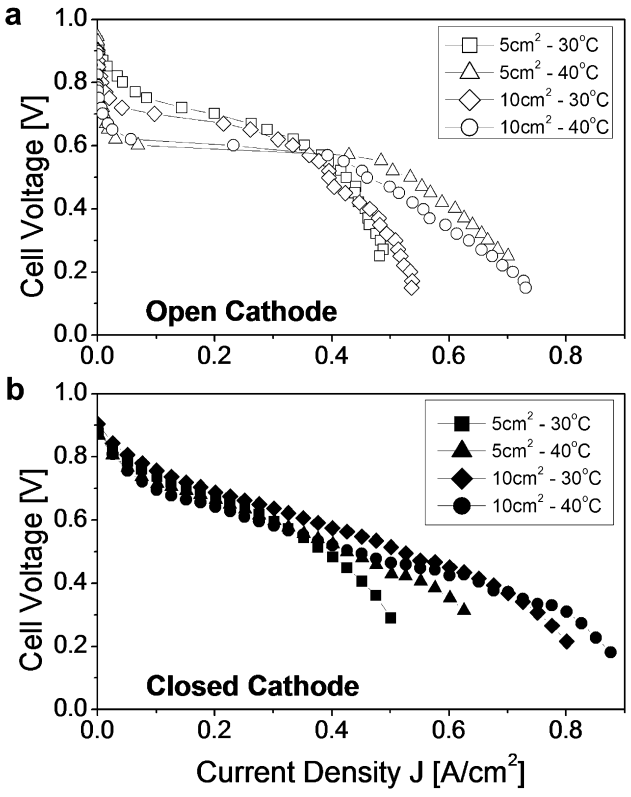

Fig. 6. Polarization curves at 30 °C and 40 °C. (a) Open cells (b) Closed cells.

4.1.3. Water droplet formation on the open-cathode

Formation of water droplets occurred at higher current densities on the GDL of the open cells. The amount of water depended on cell temperature which is consistent with the results presented by Ous and Arcoumanis [18]. An image of the water formation can be seen in Fig. 7. No visible droplets were observed above 40 °C where the rate of evaporation exceeded (or was more in balance with) the rate of water production. At 30 °C and low current densities, very small droplets of water could be seen on the exposed GDL on both the 5 cm^2 and 10 cm^2 cells. At higher current densities at 30 °C, the water droplets were significantly bigger for both cells. During the polarization testing, product water pooled at the bottom of the cathode plate slots due to the vertical orientation of the fuel cells. This flooding reduces the effective active area of the cell, and coupled with low airflow over the cell surface, is likely a major contributor to the drop-off of the 30 °C polarization curves in Fig. 6a.

Additionally, the increase in liquid water contributes to performance loss in the form of mass transport resistance by inhibiting diffusion of gasses through the GDL [16,19,20]. This effect is likely present in both open and closed cell configurations although less pronounced at 40 °C due to higher evaporation.

4.1.4. Cell power density

Although polarization curves provide general insight into the overall cell performance and behavior, in most practical applications for fuel cells, an important aspect to consider is power density. Table 1 lists the maximum power density and its corresponding current density for each cell configuration and temperature. Data for 60 °C cell temperature is not listed for the 5 cm^2 open-cathode as performance is severely limited in this case due to membrane dry out – see Fig. 5 and discussion above. From the data, it can be seen that the current density for maximum power density increases with temperature for all cases. This follows the trend seen in the potential curves where temperature increases the maximum current density achieved by each cell. From the 5 cm^2 open-cathode temperature scan, the maximum power density increases with temperature and drops after 40 °C. Although the maximum current density is greatest at 50 °C, fuel cell efficiency tends to decrease with increased temperature [13]. In each of the other cell configurations, the maximum power density increases from 30 °C to 40 °C. In general, the open cells are able to match or exceed the maximum power density produced by the closed cells. This is most likely due to the fact that under constant stoichiometry flow conditions, with respect to the closed cell, efficiency decreases with increasing current density [13].

Ultimately, the 5 cm^2 open cell operating at 40 °C produced the greatest power density. This suggests that for low power devices, an

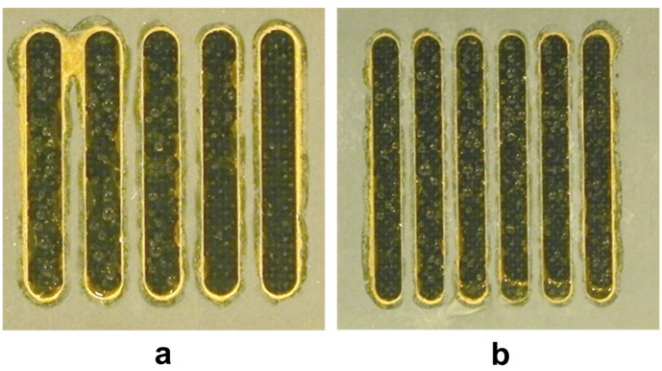

Fig. 7. Water accumulation on the GDL of open cells at 30 °C and 0.4 A/cm^2. (a) 5 cm^2 cell (b) 10 cm^2 cell.

Table 1
Maximum power generated by 5 cm^2 open cell and current density at max power for Room, 30, 40, and 50 °C respectively. Only 30 and 40 °C shown for 5 cm^2 closed and 10 cm^2.

Cell size	Max power [mW/cm^2]	J [mA/cm^2] for max P
5 cm^2 Open	168, 218, 267, 262	357, 383, 484, 654
10 cm^2 Open	188, 235	399, 500
5 cm^2 Closed	207, 224	402, 552
10 cm^2 Closed	208, 235	378, 452

H_2/Air fuel cell is best (or at least viable) in an open-cathode configuration. Again, it should be noted that the fuel cells were tested while oriented vertically and that only one airflow condition was tested in closed cell configuration.

4.2. Electrochemical impedance spectroscopy

Electrochemical impedance spectroscopy (EIS) is a valuable diagnostics tool in that it allows for the distinction between individual voltage losses at a given operating point [1]. While potential curves provide an overview of fuel cell performance, EIS helps identify which losses have the greatest effect on fuel cell performance. EIS was used to explore how temperature, cell size, and cell configuration change the influence of losses at a particular set point.

Fig. 8 shows impedance data at 0.4 A/cm^2 for each cell configuration. The data is presented as Nyquist plots – imaginary resistance versus real resistance in Ω-cm^2. The high frequency resistance (R_{hf}) is the left intercept of the real axis and represents the total Ohmic resistance of the fuel cell [11]. From the data, R_{hf} does not differ significantly between configurations (approximately 0.15 ± 0.03 Ω-cm^2).

It is difficult to compare the cell configurations specifically on size due to the fact at 0.4 A/cm^2, each configuration is at a slightly different operating point along their respective polarization curve. In analyzing the impedance data, we consider the activation, Ohmic and mass transport regions of a general polarization curve [13]. Also considered are the high to mid frequency kinetic and low frequency mass transport loops of the Nyquist curves typical of impedance data for PEM fuel cells [1,13,20].

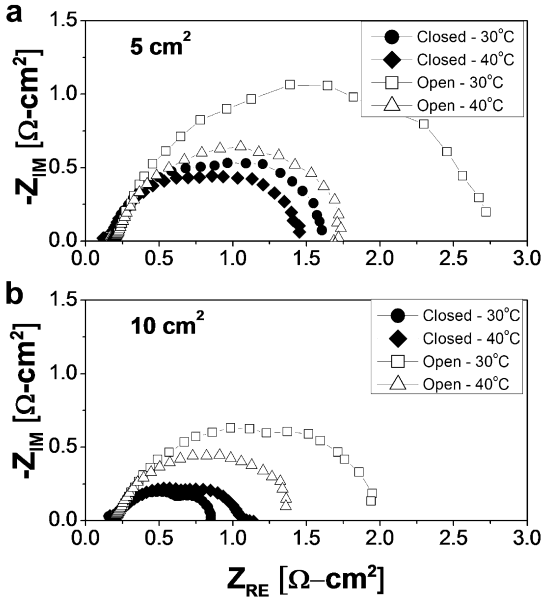

Fig. 8. Nyquist curves at 0.4 A/cm^2. (a) 5 cm^2 open and closed cathode (b) 10 cm^2 open and closed cathode.

From Fig. 6, we can see that at a current density of 0.4 A/cm^2, the open cells at 30 °C are operating in the mass transport region while at 40 °C, they are on the border between the Ohmic and mass transport regions. For the open cells, the curves are generally lumped into a single larger loop. In these configurations, it is clear that the mass transport resistance dominates and envelopes the smaller kinetic loop indicating major losses due to limited oxygen diffusion. In considering the general size of the loops between the open-cathode curves for 30 and 40 °C, the 30 °C loop is significantly larger than the 40 °C loop [16,20,21]. It is clear from this that at the lower temperatures, the fuel cell is more starved of fresh oxygen. As described in the previous section, the major factors limiting the performance at 30 °C are water accumulation and low airflow over the cell surface.

The closed cells, operating at 0.4 A/cm^2, are for the most part in the Ohmic region of the polarization with the exception of the 10 cm^2 at 40 °C which seems to be at the start of the mass transport region. In all four of these curves the kinetic and mass transport loops are more easily distinguishable from one another, especially in the cases of the 10 cm^2 closed cell [21]. Here, neither the kinetic nor the mass transport loops dominate which is unlike the cases of the open cells. The difference in magnitude between the curves at each temperature for the closed cells is also far less significant than seen with the open cells.

The impedance data helps to reinforce the results from the polarization testing. The rise in temperature to 40 °C significantly reduces losses for the open-cathode configuration. Additionally, there is not a significant change in loss magnitude between temperatures for the closed cell configuration.

5. Conclusions

The impact of temperature on air-breathing, polymer electrolyte membrane (PEM) fuel cells was investigated using polarization scans and impedance spectroscopy. Testing of a 5 cm^2 open-cathode fuel cell revealed that performance at high current densities was enhanced with increased cell temperature as the heated, more buoyant air surrounding the cell allowed for more airflow over the active membrane. The opposite was true for low current densities where performance decreased with higher temperatures as a result of membrane dry out. Maximum cell power density increased with temperature until it reached a peak at 40 °C and then dropped off with greater temperature. Performance showed a large dependence on cell temperature for the open cells while temperature and size effects were more balanced for the closed cells. The EIS data reinforces the fact that at higher temperatures, the open cell mass transport losses are much smaller as more buoyant air supplies an increased amount of fresh air to the fuel cell. Testing at 40 °C and above showed no formation of visible water droplets at the cathode surface. In this case the rate of evaporation was more balanced with the rate of water production. At 30 °C, pooling of water droplets at the bottom of the open-cathode slots decreased the effective cell active area. The 25 cm^2 open-cathode fuel cell experienced self-heating beyond the cell temperature set points of 30 °C and 40 °C. While exploring the self-heating was not the purpose of this study the extended polarization curve for the 25 cm^2 open cell illustrates the potential benefit of self-heating.

As a general statement, the data shows that the open cells are able to rival the closed cells in terms of maximum power density for the flow conditions that were tested. The 5 cm^2 open cell produced the highest power density at 40 °C. This result suggests that for low power devices, an open-cathode fuel cell is a viable option for the future. A practical ABPEM fuel cell should be designed for a specific

operating point. This would allow for the design and construction of the cell body to have proper heat rejection in order to maintain a desired steady temperature. This temperature should be chosen to maximize airflow across the fuel cell surface while also maintaining proper water content on the membrane.

Acknowledgements

We are grateful to Dr. Scott C. Barton in the Department of Chemical Engineering & Material Science at Michigan University for many discussions. Collaborative effort of Prof. Kim in Korea was made possible through the International Collaboration Grant (Grant# UD080050GD).

References

[1] E. Barsoukov, J. Macdonald, Impedance Spectroscopy: Theory, Experiment, and Applications. John Wiley and Sons, 2005.
[2] C. Dyer, Fuel cells for portable applications, Journal of Power Sources 106 (2002).
[3] L. Carrette, K.A. Friedrich, U. Stimming, Fuel cells – fundamentals and applications, Fuel Cells 1 (2001) 5–39.
[4] B.P.M. Rajani, A.K. Kolar, A model for a vertical planar air breathing PEM fuel cell, Journal of Power Sources 164 (2007) 210–221.
[5] M.A.R. Sadiq Al-Baghdadi, Performance comparison between airflow-channel and ambient air-breathing PEM fuel cells using three-dimensional computational fluid dynamics models, Renewable Energy 34 (2009) 1812–1824.
[6] M. Paquin, L.G. Fréchette, Understanding cathode flooding and dry-out for water management in air breathing PEM fuel cells, Journal of Power Sources 180 (2008) 440–451.
[7] Y. Wang, M. Ouyang, Three-dimensional heat and mass transfer analysis in an air-breathing proton exchange membrane fuel cell, Journal of Power Sources 164 (2007) 721–729.
[8] S.U. Jeong, E.A. Cho, H.-J. Kim, T.-H. Lim, I.-H. Oh, S.H. Kim, Effects of cathode open area and relative humidity on the performance of air-breathing polymer electrolyte membrane fuel cells, Journal of Power Sources 158 (2006) 348–353.
[9] M. Ay, A. Midilli, I. Dincer, Exergetic performance analysis of a PEM fuel cell, International Journal of Energy Research 30 (2006) 307–321.
[10] R. O'Hayre, T. Fabian, S. Litster, F.B. Prinz, J.G. Santiago, Engineering model of a passive planar air breathing fuel cell cathode, Journal of Power Sources 167 (2007) 118–129.
[11] T. Fabian, J. Posner, R. O'Hayre, S. Cha, J. Eaton, F. Prinz, J. Santiago, The role of ambient conditions on the performance of a planar, air-breathing hydrogen PEM fuel cell, Journal of Power Sources 161 (2006) 168–182.
[12] T. Hottinen, M. Noponen, T. Mennola, O. Himanen, M. Mikkola, P. Lund, Effect of ambient conditions on performance and current distribution of a polymer electrolyte membrane fuel cell, Journal of Applied Electrochemistry 33 (2003) 265–271.
[13] R. O'hayre, S. Cha, W. Colella, F. Prinz, Fuel Cell Fundamentals. John Wiley & Sons, 2006.
[14] J.-H. Koh, A.T. Hsu, H.U. Akay, M.-F. Liou, Analysis of overall heat balance in self-heated proton-exchange-membrane fuel cells for temperature predictions, Journal of Power Sources 144 (2005) 122–128.
[15] Y. Zhang, R. Pitchumani, Numerical studies on an air-breathing proton exchange membrane (PEM) fuel cell, International Journal of Heat and Mass Transfer 50 (2007) 4698–4712.
[16] T.E. Springer, T.A. Zawodzinski, M.S. Wilson, S. Gottesfeld, Characterization of polymer electrolyte fuel cells using AC impedance spectroscopy, Journal of the Electrochemical Society 143 (1996) 587–599.
[17] S. Wasterlain, D. Candusso, D. Hissel, F. Harel, P. Bergman, P. Menard, M. Anwar, Study of temperature, air dew point temperature and reactant flow effects on proton exchange membrane fuel cell performances using electrochemical spectroscopy and voltammetry techniques, Journal of Power Sources 195 (2010) 984–993.
[18] T. Ous, C. Arcoumanis, The formation of water droplets in an air-breathing PEMFC, International Journal of Hydrogen Energy 34 (2009) 3476–3487.
[19] H. Li, Y. Tang, Z. Wang, Z. Shi, S. Wu, D. Song, J. Zhang, K. Fatih, J. Zhang, H. Wang, Z. Liu, R. Abouatallah, A. Mazza, A review of water flooding issues in the proton exchange membrane fuel cell, Journal of Power Sources 178 (2008) 103–117.
[20] X. Yuan, C. Song, H. Wang, J. Zhang, Electrochemical Impedance Spectroscopy in PEM Fuel Cells: Fundamentals and Applications. Springer Verlag, 2009.
[21] X. Yuan, H. Wang, J. Colin Sun, J. Zhang, AC impedance technique in PEM fuel cell diagnosis—a review, International Journal of Hydrogen Energy 32 (2007) 4365–4380.